JGR Atmospheres

RESEARCH ARTICLE
10.1029/2024JD042943

The Impact of 2022 Hunga Tonga-Hunga Ha'apai (Hunga) Eruption on Stratospheric Circulation and Climate

Simchan Yook[1], **Susan Solomon**[1], **and Xinyue Wang**[2]

[1]Department of Earth, Atmospheric and Planetary Sciences, Massachusetts Institute of Technology, Cambridge, MA, USA, [2]Department of Atmospheric and Oceanic Sciences, University of Colorado Boulder, Boulder, CO, USA

Key Points:

- Simulated climate responses to the Hunga eruption based on specified-chemistry runs show good agreement with previous coupled-chemistry runs
- Ozone, water vapor, and aerosol from the Hunga eruption each contributed to the circulation and temperature anomalies in the stratosphere
- The simulated springtime ozone anomalies contributed to the temperature anomalies in the Southern Hemisphere lower stratosphere during winter 2022

Correspondence to:
S. Yook,
syook@mit.edu

Citation:
Yook, S., Solomon, S., & Wang, X. (2025). The impact of 2022 hunga tonga-hunga ha'apai (hunga) eruption on stratospheric circulation and climate. *Journal of Geophysical Research: Atmospheres*, *130*, e2024JD042943. https://doi.org/10.1029/2024JD042943

Received 14 NOV 2024
Accepted 2 MAR 2025

Abstract The Hunga Tonga-Hunga Ha'apai (Hunga) volcanic eruption in January 2022 injected a substantial amount of water vapor and a moderate amount of SO_2 into the stratosphere. Both satellite observations in 2022 and subsequent chemistry-climate model simulations forced by realistic Hunga perturbations reveal large-scale cooling in the Southern Hemisphere (SH) tropical to subtropical stratosphere following the Hunga eruption. This study analyzes the drivers of this cooling, including the distinctive role of anomalies in water vapor, ozone, and sulfate aerosol concentration on the simulated climate response to the Hunga volcanic forcing, based on climate simulations with prescribed chemistry/aerosol. Simulated circulation and temperature anomalies based on specified-chemistry simulations show good agreement with previous coupled-chemistry simulations and indicate that each forcing of ozone, water vapor, and sulfate aerosol from the Hunga volcanic eruption contributed to the circulation and temperature anomalies in the SH stratosphere. Our results also suggest that (a) the large-scale stratospheric cooling during the austral winter was mainly induced by changes in dynamical processes, not by radiative processes, and that (b) the radiative feedback from negative ozone anomalies contributed to the prolonged cold temperature anomalies in the lower stratosphere (~70 hPa level) and hence to long lasting cold conditions of the polar vortex.

Plain Language Summary In January 2022, the Hunga Tonga-Hunga Ha'apai (Hunga) volcanic eruption injected large amounts of water vapor and moderate amounts of sulfur dioxide into the stratosphere. Previous observational and modeling studies show that this injection led to decreases in stratospheric temperature. We use a climate model forced with prescribed chemical composition from the Hunga eruption to explore how the changes in water vapor, ozone, and sulfate aerosols affected stratospheric climate. Our findings confirm that these forcings all contributed to the changes in temperatures and circulation in the SH's stratosphere. The cooling during austral winter was mainly due to changes in atmospheric dynamics rather than direct radiative effects, but the ozone's radiative feedback also contributed to sustaining the cold temperature anomalies in the lower stratosphere in late spring.

1. Introduction

The Hunga Tonga-Hunga Ha'apai (Hunga) volcanic eruption (21°S, 175°W) was one of the most explosive eruptions observed since the satellite era. Observations reveal that the Hunga eruption injected a substantial amount of water vapor (>150 Tg) into the stratosphere, resulting in a ~10% increase in the stratospheric water vapor burden (Khaykin et al., 2022; Millán et al., 2022; Vömel et al., 2022), which was unprecedented in the available observational record. The Hunga eruption also injected a moderate amount of SO_2 (~0.4–0.5 Tg) into the stratosphere (Carn et al., 2022; Sellitto et al., 2022; Taha et al., 2022; Witze, 2022). The injected SO_2 was quickly converted to sulfate aerosol particles through oxidation, which was accelerated by the excessive moisture (Asher et al., 2023; Wang et al., 2023; Zhu et al., 2022).

Many studies have explored the impacts of the Hunga water vapor and aerosol perturbations on stratospheric temperatures, circulation and chemistry. Both satellite observations in 2022 and subsequent model simulations forced by realistic Hunga perturbations reveal large-scale cooling in the Southern Hemisphere (SH) tropical to subtropical stratosphere, large mesospheric temperature anomalies (Yu et al., 2023), a strengthening and equatorward shift of the stratospheric polar night jet, and a weaker stratospheric overturning circulation (Coy et al., 2022; Fleming et al., 2024; Schoeberl et al., 2022; Wang et al., 2023). Substantial ozone reduction was also observed in the mid-stratosphere over SH mid-latitudes during austral winter and over polar regions during austral spring (Lu et al., 2023; Wang et al., 2023; Zhang et al., 2024). The net tropospheric radiative forcing from the

Hunga perturbations is estimated to be small but negative due to compensation between a heating linked to the water vapor increase and a cooling due to the reduction in direct solar flux by the aerosol layer (Schoeberl et al., 2023).

The changes in stratospheric composition and circulation in response to the Hunga forcing evolve through complex interactions in the atmosphere. This complexity makes it challenging to quantify the exact role of each forcing on climate anomalies in a coupled chemistry-climate model simulation. For example, the evolution of ozone is simulated through both dynamical and chemical processes in a coupled chemistry model. The changes in ozone can affect temperatures and thus circulation through radiative effects, which, in turn, can affect the ozone concentration again. Thus, in a coupled chemistry simulation, it is difficult to quantify to what extent the circulation anomalies in 2022 were forced by the ozone perturbations. Additionally, while some single forcing (e.g., water vapor or SO_2 only) experiments can be conducted in the coupled chemistry-climate setting to separate the role of each Hunga volcanic forcing on the climate responses, they require assumptions that any differences in the evolution of water vapor and SO_2 among different experiments are negligible. Thus, making a precise attribution of each forcing on the circulation anomalies in the coupled chemistry simulation is difficult.

Wang et al. (2023) conducted comprehensive analyses using coupled chemistry-climate simulations forced by realistic Hunga inputs of H_2O and SO_2. Their simulations successfully reproduced the observed changes in temperature, circulation, and ozone, demonstrating how the Hunga forcing contributed to the stratospheric climate anomalies and ozone losses in 2022. Here we conduct further analysis aimed at identifying the contribution of each individual forcing term that contributes to those climate anomalies: ozone, water vapor, and aerosols, respectively. To do so, we ran a series of numerical experiments using the "Specified Chemistry" (SC) version of the Whole Atmosphere Community Climate Model (WACCM; Gettelman et al., 2019) forced with prescribed chemical composition from the previous "Free Running" (FR) WACCM simulations by Wang et al. (2023).

2. Method

2.1. SC-WACCM

To isolate the circulation responses to the Hunga perturbations from the coupled chemistry-climate interactions, we used the SC version of the WACCM (SC-WACCM; Smith et al., 2014). The SC-WACCM simulations were run with a horizontal resolution of $1.25° \times 0.9°$, 70 vertical levels, and a model top at about 140 km. The model was coupled to interactive ocean, land, and sea ice models.

The SC-WACCM simulation is essentially identical to the FR-WACCM simulation except that the chemical composition of the middle atmosphere is prescribed as data, rather than calculated by the model (details described in Smith et al., 2014). SC-WACCM simulates only the radiative effects of prescribed concentrations of gases and aerosols on the temperature fields, but not the influence of dynamical fields on the chemical species. Thus, using SC-WACCM, we can estimate the circulation responses to specified amounts of gas and aerosol perturbations in a consistent manner across various sets of experiments. For example, sulfate aerosol in the SO_2-only experiment run on the FR-WACCM simulations may not be identical to the aerosol in the FR-WACCM simulations run with both SO_2 and H_2O forcing due to differences in the dynamical and chemical evolution of the sulfate aerosol between the two runs. However, in SC-WACCM, we can apply the same aerosol forcing for different sets of experiments. Since SC-WACCM does not involve any calculations of chemical reactions, it can also reduce computational costs to about half of those for the FR-WACCM, while reproducing similar results in long-term statistics of climate scale (Smith et al., 2014).

2.2. Experiments

We used two sets of FR-WACCM experiments conducted by Wang et al. (2023) to generate the prescribed chemical composition forcing files and compare the results: (a) **FR-CTRL**, the control case run without the Hunga volcanic forcing, and (b) **FR-ALL**, the perturbed case run with realistic Hunga forcing. The Hunga volcanic forcing in the **FR-ALL** runs included the injection of 150 Tg of H_2O and 0.42 Tg of SO_2 into the stratosphere (for details, see Section 2.3 in Wang et al., 2023). In parallel with their FR-WACCM simulations, we performed five sets of additional SC-WACCM experiments forced with different combinations of prescribed chemical compositions (water vapor, ozone, and aerosol) as follows:

(a) **SC-CTRL**, control experiments forced with the water vapor, ozone, and aerosol fields taken from the **FR-CTRL** runs,

(b–d) **SC-H2O**, **SC-O3**, and **SC-SULF**, three sets of single forcing experiments forced with water vapor, ozone, and sulfate aerosol field, respectively, from the **FR-ALL** runs and two other fields from the **FR-CTRL** runs, and

(e) **SC-ALL**, all forcing experiments forced with all three fields from the **FR-ALL** runs.

The forcing files were generated based on zonal-mean and daily mean fields from each ensemble member. We used 10 ensemble members for each set of experiments, each run with forcing files generated from the corresponding ensemble member of the FR runs, to isolate the circulation responses to the Hunga forcing from other forms of internal climate variability. All ensemble members were integrated from 1 January 2022, until 31 December 2022.

To reproduce the initial structure and development of the Hunga plume, the modeled winds and temperatures were relaxed toward reference meteorology from Modern-Era Retrospective Analysis for Research and Applications version 2 (MERRA2, Gelaro et al., 2017). Following Wang et al. (2023), in all experiments we adjusted the WACCM wind and temperature fields to match the MERRA2 data with a relaxation time of 12 hr throughout January 2022. After 1 February 2022, the model was free-running without any nudging applied.

The differences in ensemble mean fields between the forcing and control runs are explored to estimate the mean climate anomalies in response to the Hunga forcing. The t-statistic was used to assess the statistical significance of the difference ($p < 0.05$) in mean climate between two sets of simulations. The main purpose of this study was to examine the climate response to the chemical forcing derived from the previous FR-WACCM simulations. Thus, we compared the results from the SC runs with those from the FR runs, rather than with observations.

2.3. Ozone Monitor and Profiler Suite Limb Profiler (OMPS)

The ozone anomaly data for 2022 (with respect to the 2012–2021 mean seasonal cycle) were derived from the Ozone Mapping and Profiler Suite Limb Profiler instrument (Taha et al., 2021; Zawada et al., 2018). Ozone Monitor and Profiler Suite Limb Profiler (OMPS) observations have been employed in multiple studies investigating the Antarctic ozone hole (Kramarova et al., 2014; Rieger et al., 2021; Wang et al., 2023; Yu et al., 2021). We note that the OMPS ozone data were used to compare the modeled evolution of ozone with observations but not used as prescribed forcing in the model experiments.

3. Results

The Hunga perturbations in the **FR-ALL** simulations consist of stratospheric aerosol and gases that evolve over time following the initial injection of SO_2 and H_2O into the stratosphere. Wang et al. (2023) demonstrated that the simulated evolution of the H_2O and sulfate aerosol plumes, resulting from the initial perturbations, closely matches the patterns from satellite observations. We hypothesized that water vapor, ozone, and sulfate aerosol were the main radiative forcings resulting from the initial injection of the Hunga forcing. Thus, we used the water vapor, ozone, and sulfate aerosol fields from the **FR-ALL (FR-CTRL)** experiments to form the prescribed Hunga forcing in the **SC-ALL (SC-CTRL)** experiments.

We assess whether the simulated circulation and temperature anomalies from the SC-WACCM runs, forced with prescribed stratospheric water vapor, ozone, and aerosols, align well with the results from the FR-WACCM runs. Figure 1 shows the temperature responses (averaged over 50°S–0°S) to the Hunga forcing as differences between the all forcing (**ALL**) runs and the control (**CTRL**) runs in FR- and SC-WACCM simulations (top and bottom, respectively). Consistent with findings from previous studies (Fleming et al., 2024; Wang et al., 2023), the Hunga perturbations lead to cooling of ∼1 K over much of the middle stratosphere above ∼30 hPa level, juxtaposed with weaker warming in the lower stratosphere below ∼50 hPa throughout 2022, in both the FR and SC runs (Figure 1). Close similarity in the climate responses to the Hunga perturbations between the FR and SC runs shown in Figure 1 suggests that (a) the three forcings in SC runs effectively represent the net radiative forcing of the Hunga perturbations, and (b) the simulated SH temperature anomalies in the stratosphere during 2022 are radiative responses to the Hunga forcing.

We next explore the extent to which the climate anomalies in 2022 were affected by each forcing of ozone, water vapor, and sulfate aerosol from the Hunga eruption. Figure 2 reveals the temperature anomalies based on the single forcing experiments, **SC-H2O**, **SC-O3**, and **SC-SULF**. The temperature anomalies based on single forcing

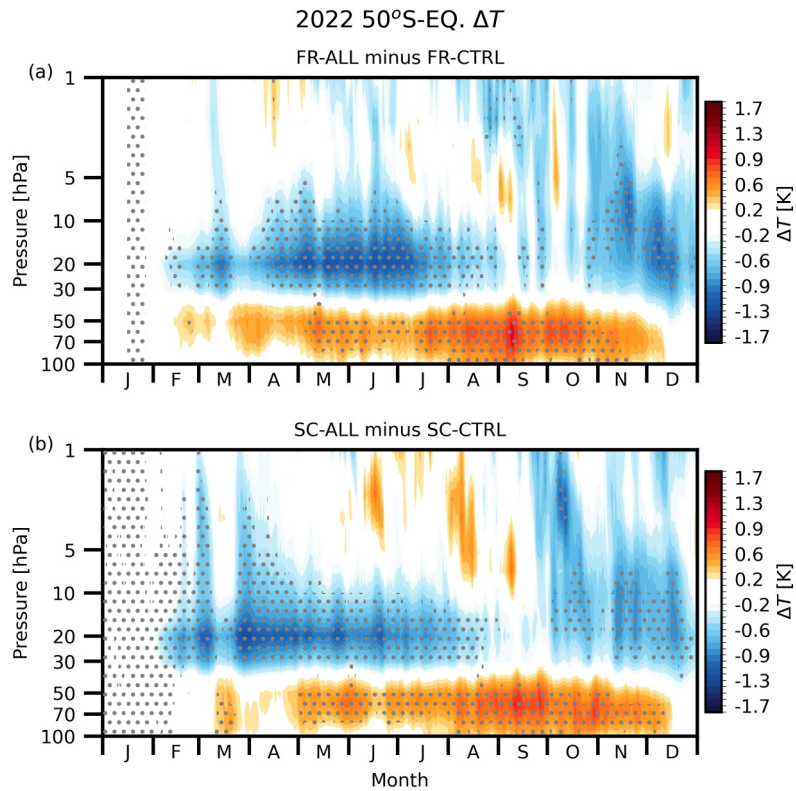

Figure 1. Time evolution of differences in temperature averaged over 50°S–0°S between all forcing (ALL) and control (CTRL) runs, based on (a) FR, and (b) SC runs, respectively. Stippling indicates statistical significance at the 95% confidence level.

experiments show that the persistent cold temperature anomalies above ~30 hPa level are largely due to the water vapor perturbations (Figures 1 and 2a). This is expected, as the radiative effects of stratospheric water vapor will induce cooling in the stratosphere (Forster and Shine, 1999). Wang et al. (2023) also showed that the cold temperature anomalies overlap with the water vapor plume. The warm temperature anomalies below the ~30 hPa level result from radiative heating from the volcanic aerosol layer in the lower stratosphere. These warm anomalies are reinforced by the absorption of upwelling longwave radiation by the water vapor plume (Figures 2a and 2c, and also Figure 3 in Wang et al., 2023).

In the following section, we explore the wintertime circulation and temperature anomalies. Figure 3 reveals the difference in wintertime (July–August–September) zonal-mean temperature (top) and zonal wind (bottom) between the all forcing (**ALL**) runs and the control (**CTRL**) runs in (left) FR- and (right) SC-WACCM simulations. The simulated temperature differences show a cooling pattern in the stratosphere centered at extratropical latitudes ~60°S in both the FR and SC runs (Figures 3a and 3b). The zonal wind anomalies also reveal a strengthening of the equatorward flank of the winter westerlies in both runs (Figures 3c and 3d).

However, unlike the substantial cooling pattern that emerges at high latitudes, the water vapor driven cooling anomalies at tropical latitudes (above 30 hPa), discussed in the previous section, become less distinct during August–October in the **SC-ALL** runs (Figures 1 and 3). Given that cold temperature anomalies are observed at extratropical latitudes during the austral winter (Figure 3), we expect dynamically induced warming over the tropics due to the well-known out-of-phase temperature variations between the tropics and extratropics, associated with changes in the Brewer-Dobson circulation (Randel et al., 2007; Ueyama & Wallace, 2010; Yulaeva et al., 1994). The signatures of a warming pattern over the tropics, coupled with the cooling over the extratropics, are also evident in the **SC-SULF** runs, where the tropical cooling from the water vapor anomalies is absent (Figures 2c and 4d). Thus, we infer that the dynamical coupling of wintertime circulation between the extratropics and tropics induces warming over the tropics which partially offsets the radiative cooling caused by the water vapor forcing in **SC-ALL** runs (Figures 1 and 3).

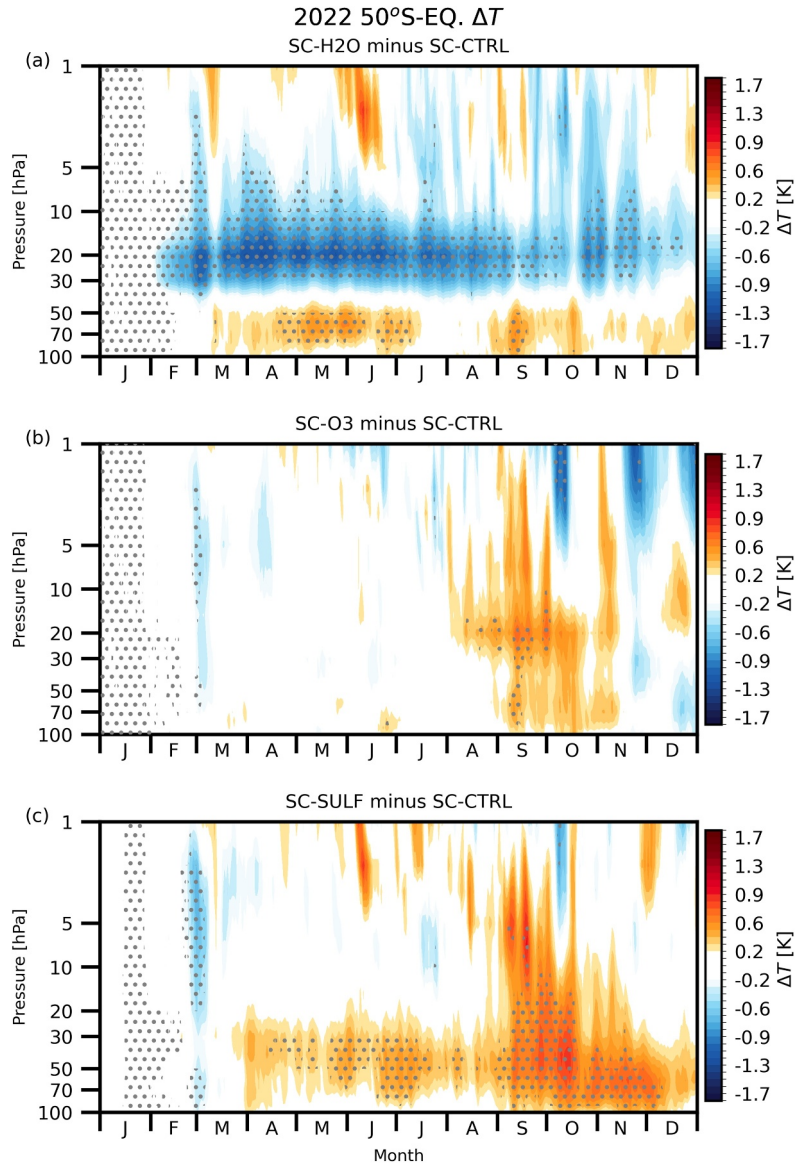

Figure 2. As in Figure 1, but for differences between (a) SC-H2O and SC-CTRL, (b) SC-O3 and SC-CTRL, and (c) SC-SULF and SC-CTRL runs.

Figure 4 presents the wintertime circulation anomalies from the three single forcing experiments, showing the differences between each of the three forcing runs (**SC-H2O**, **SC-O3**, and **SC-SULF**) and the **SC-CTRL** runs. The single forcing runs exhibit a similar pattern of wintertime climate anomalies, including cooling of the Antarctic polar vortex and a strengthening of the equatorward flank of the stratospheric polar jet, consistent with the all forcing runs.

The **SC-SULF** runs exhibit the largest zonal wind and temperature anomalies among the three single-forcing experiments (Figure 4). Aerosols from large tropical volcanic eruptions can influence stratospheric temperatures and winds through direct radiative effects (e.g., DallaSanta et al., 2019; Kodera, 1994; Robock, 2000; Robock & Mao, 1995; Toohey et al., 2014) and indirect mechanisms (e.g., Coupe & Robock, 2021). Previous modeling studies have also shown that direct warming in the tropical stratosphere leads to the strengthening of the winter polar vortex (e.g., DallaSanta et al., 2019; Revell et al., 2017; Toohey et al., 2014). In the **SC-SULF** runs, warm temperature anomalies are observed in the lower tropical stratosphere due to radiative heating from the volcanic aerosol layer (Figures 2c and 4c). Thus, consistent with findings from other modeling studies, the

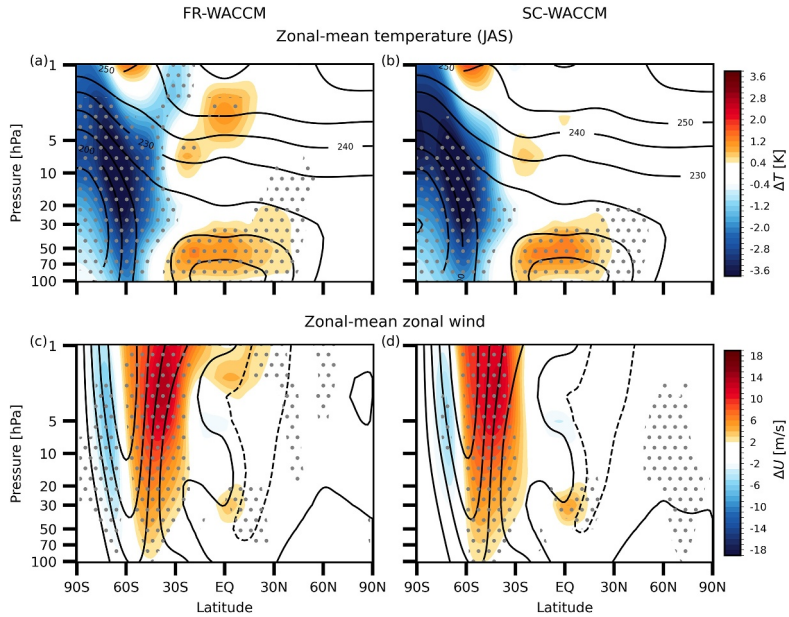

Figure 3. Differences in zonal-mean (top) temperature and (bottom) zonal wind fields between all-forcing (ALL) and control (CTRL) runs. The results are based on (left) FR and (right) SC runs, respectively. Black line contours are spaced at 180, 190, 200… K for the mean temperature, and −40, −20, 0… m/s for the mean zonal wind from CTRL experiments. The results are averaged during the austral winter, from July–September 2022.

wintertime climate anomalies in the **SC-SULF** runs indicate the response to lower tropical warming induced by the aerosol layer (Figures 4c and 4f).

However, we note that the extratropical circulation anomalies in the single-forcing experiments have much smaller amplitudes compared to those in the all-forcing runs (Figures 3 and 4) and are not statistically significant ($p > 0.05$). Thus, including both water vapor and sulfate aerosol forcings is expected to be important for a realistic simulation of the Hunga forcing.

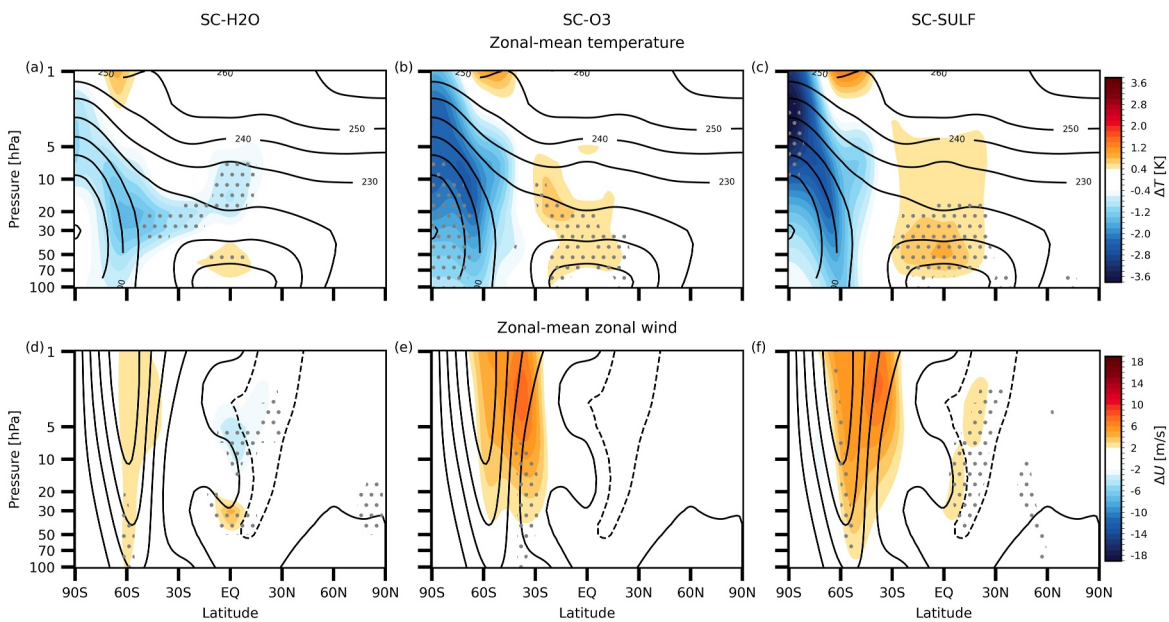

Figure 4. As in Figure 3, but for results based on (a), (d) SC-H2O minus SC-CTRL, (b), (e) SC-O3 minus SC-CTRL, and (c), (f) SC-SULF minus SC-CTRL.

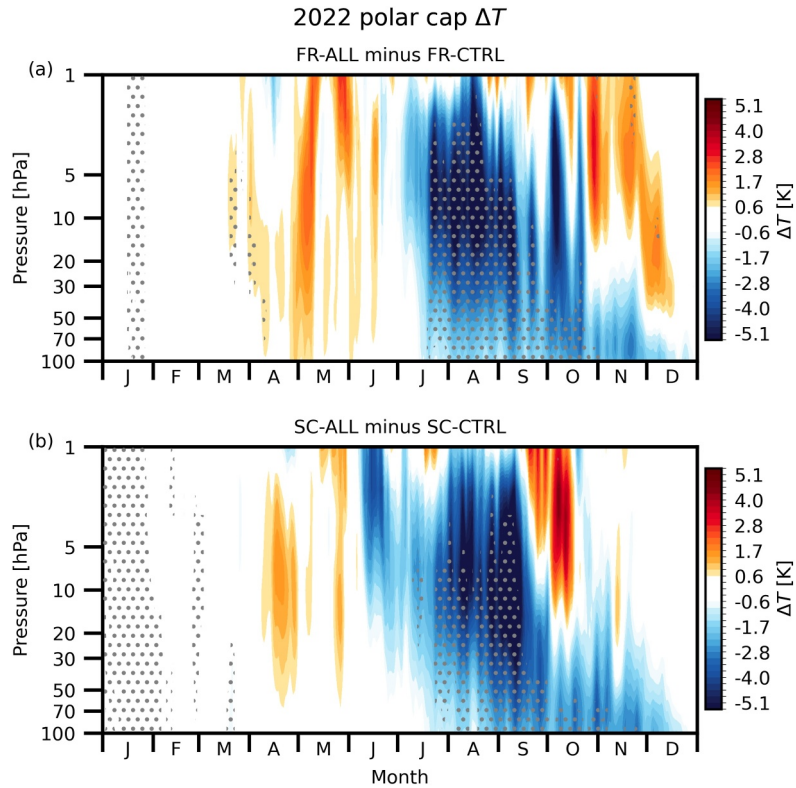

Figure 5. As in Figure 1, bur for Southern Hemisphere polar cap-averaged (60°S–90°S) temperature. The results are based on (a) FR and (b) SC runs.

It is also known that the circulation response can be obscured by the large internal variability of the stratospheric polar vortex (DallaSanta & Polvani, 2022). Dynamical analyses based on the FR runs by Yu et al. (2023) and Wang et al. (2023) also suggest a considerable contribution of stochastic components in the wintertime extratropical circulation response to the Hunga eruption. Thus, while the similarity between the circulation anomalies in the FR and SC runs (Figure 3) provides circumstantial evidence that the wintertime circulation anomalies are likely due to the Hunga eruption, we also note that considerable stochastic variability remains due to the limited number of available ensemble members.

To better understand the wintertime climate responses to the Hunga forcing, the time series of daily mean polar cap averaged (60°S–90°S) temperature anomalies are illustrated in Figure 5. Given the low signal-to-noise ratio observed in the wintertime circulation anomalies from the single forcing experiments (Figure 4), we focus on the results based on all forcing experiments. The vertical structure of the polar cap temperature responses both in the FR and SC runs shows a similar cooling pattern across most of the stratosphere during the austral winter and spring 2022, with the largest cold anomalies in August-September (Figure 5). Extratropical winds are in thermal wind balance with the temperature anomalies. Thus, the pattern of extratropical (30°S–60°S) zonal mean zonal wind anomalies is illustrated in Figure 6. The intensification of the extratropical zonal mean zonal winds is shown throughout the stratosphere during winter, extending into the lower stratosphere in spring (Figure 6). We note that the SC runs do not show significant tropospheric or surface temperature anomalies in 2022 (not shown).

We further assess the contribution of radiative and dynamical processes to the simulated polar cap averaged (60°S–90°S) temperature anomalies focusing on the results from the SC-WACCM experiments (**SC-ALL** minus **SC-CTRL**) in Figure 7. The polar cap temperature anomalies at the upper (5 hPa) and lower (70 hPa) stratospheric levels are decomposed into three components: shortwave (SW) heating rates, longwave (LW) heating rates, and dynamical temperature changes, in Figures 7a and 7b, respectively. The temperature tendencies from different dynamical and physical processes are derived from the output fields in Community Earth System Model: DTCORE for tendency driven by dynamical processes (i.e., the temperature tendency calculated by the dynamical core), QRL for longwave heating, and QRS for shortwave heating. Other physical processes (e.g., vertical

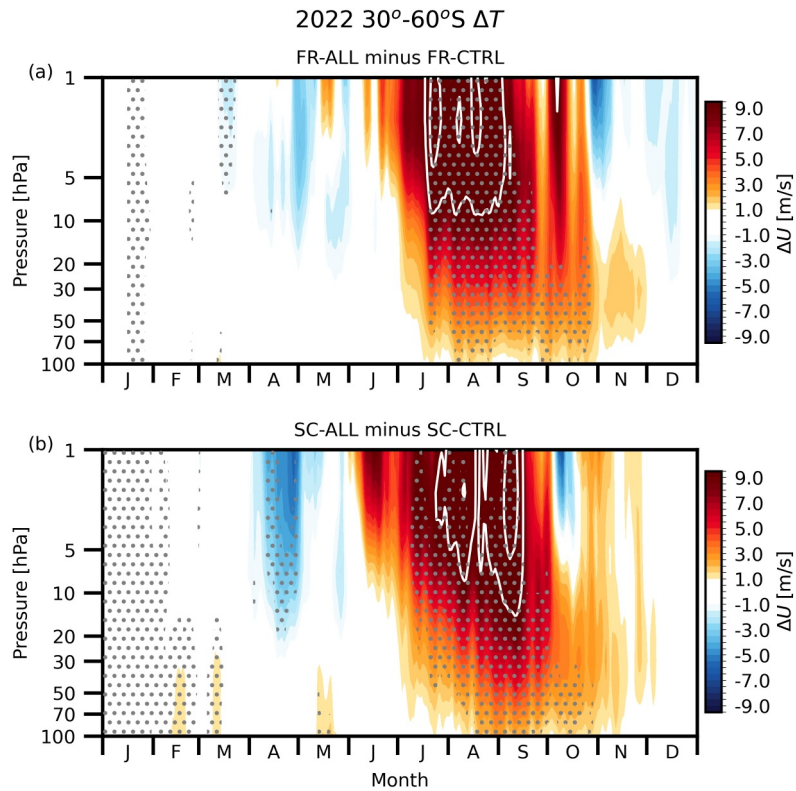

Figure 6. As in Figure 5, but for zonal-wind in the Southern Hemisphere mid-latitudes (30°S–60°S). White contour lines indicate regions where zonal wind anomalies exceed 10 m/s, with intervals of 5 m/s. The results are based on (a) FR and (b) SC runs.

diffusion, gravity wave drag, and moisture processes) also contribute to temperature changes. However, their effects were negligible in our analyses, which focused on the differences between the **SC-ALL** and **SC-CTRL** experiments.

The results shown in Figure 7 are not a time series of temperature tendencies (units: K/sec), but time-integrated temperature tendencies (units: K) since 1 January 2022. The time integration of temperature tendencies enables us to directly compare the temperature changes calculated from each temperature tendency with the temperature anomalies shown in Figure 5. The same method was used in Zou et al. (2021) for their temperature diagnosis.

Cold temperature anomalies in the upper stratosphere begin to develop in early June (with the onset indicated by the gray line), primarily due to enhanced dynamical cooling, partially offset by decreased longwave cooling from the reduced Planck feedback (Figure 7a). These changes in dynamical temperature tendencies are consistent with findings in previous studies (Coy et al., 2022; Wang et al., 2023), which indicate that the wintertime circulation responses to the Hunga forcing are characteristic of dynamically forced effects, including weakened planetary-scale wave forcing and changes in the residual mean (Brewer-Dobson) circulation.

Interestingly, while dynamical cooling drives the cold temperature anomalies in the lower stratosphere (70 hPa) during June–November, a comparable amount of negative anomalies in shortwave heating also contribute to the prolonged cold temperature anomalies during October–December (Figure 7b). We identify the source of these SW heating anomalies by comparing the SW heating anomalies in the all forcing (**SC-ALL**) and ozone-only forcing (**SC-O3**) experiments in Figure 8. The results from the **SC-ALL** and **SC-O3** runs reveal a consistent pattern of changes in shortwave heating rates, including substantial negative anomalies in the lower stratosphere during October–December (Figure 6). However, no significant changes in SW heating rates are observed in the **SC-SULF** and **SC-H2O** runs (not shown). This suggests that the SW heating anomalies in the lower stratosphere in late spring are largely driven by the radiative effects of ozone. The results are also consistent with findings from

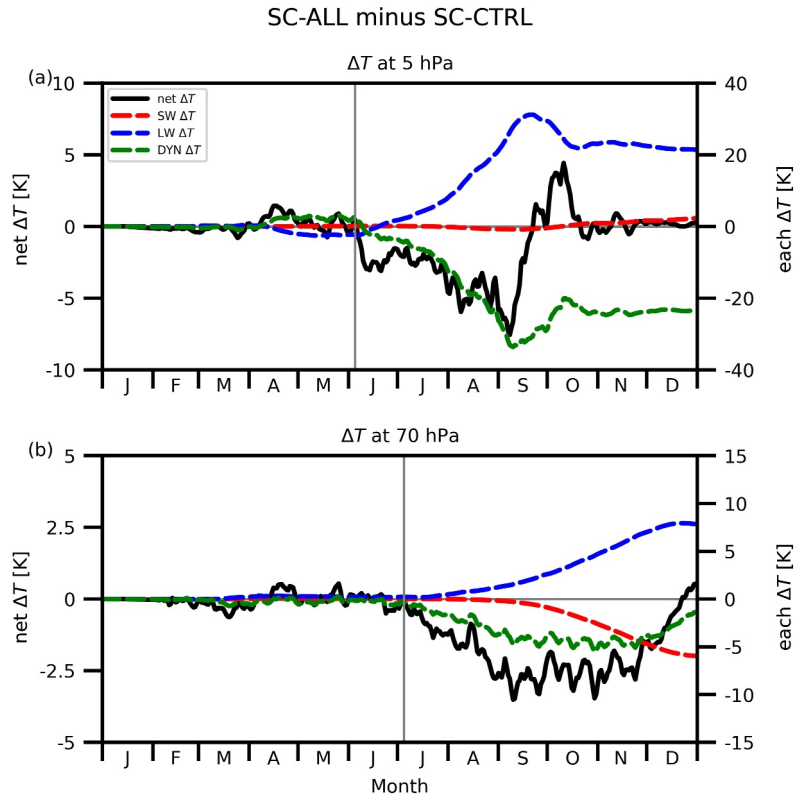

Figure 7. Time evolution of polar cap-averaged (60°S–90°S) temperature at (a) 5 hPa, and (b) 70 hPa level. Black solid line represents net temperature change (net ΔT) since 1 January 2022. Dashed lines show contribution from each of short-wave (red; SW ΔT), long-wave (blue; LW ΔT), and dynamical (green; DYN ΔT) processes. All results represent difference between SC-ALL and SC-CTRL runs. The left *y*-axis corresponds to the net ΔT, while the right *y*-axis corresponds to the magnitude of each contribution. Gray line indicates the onset of cold temperature anomalies and is defined as the first day when the sign of the net ΔT changes to negative, with the negative ΔT value sustained for at least the next 90 days.

previous studies suggesting that ozone changes are the primary driver of temperature changes in the lower stratosphere during austral spring (Calvo et al., 2012, 2017).

Figure 9 shows the evolution of springtime polar-cap ozone anomalies in 2022 based on OMPS observations (top) and simulated ozone from FR-WACCM (bottom). Both the observations and the WACCM simulations show negative anomalies in polar-cap ozone concentrations across much of the stratosphere during spring 2022. Zhang et al. (2024) reported that most of the ozone anomalies in 2022 were primarily driven by circulation anomalies. However, their findings also show that the chemical loss of ozone was particularly large in the lower stratosphere during austral spring 2022, accounting for up to ∼20% of the Antarctic ozone loss at 80 hPa in October 2022. Thus, together with the findings from Zhang et al. (2024), the results in Figures 8 and 9 emphasize the role of chemistry-climate interactions in driving climate anomalies in the lower stratosphere. We note that the occurrence of positive ozone anomalies above the negative ozone anomalies is consistent with the signatures of dynamical changes investigated in previous studies (Calvo et al., 2012, 2017).

4. Summary and Conclusions

Recent observational and modeling studies explored the stratospheric climate anomalies following the Hunga volcanic eruption, including influences on the stratospheric temperatures, chemistry, large-scale circulation, and net radiative forcing (Coy et al., 2022; Fleming et al., 2024; Lu et al., 2023; Schoeberl et al., 2022, 2023; Wang et al., 2023; Zhang et al., 2024). Two recent studies used the same chemistry-climate model (WACCM) but with different configurations to address various aspects of the climate responses to the Hunga eruption. Wang et al. (2023) explored the evolution of stratospheric composition and circulation using a free-running version of

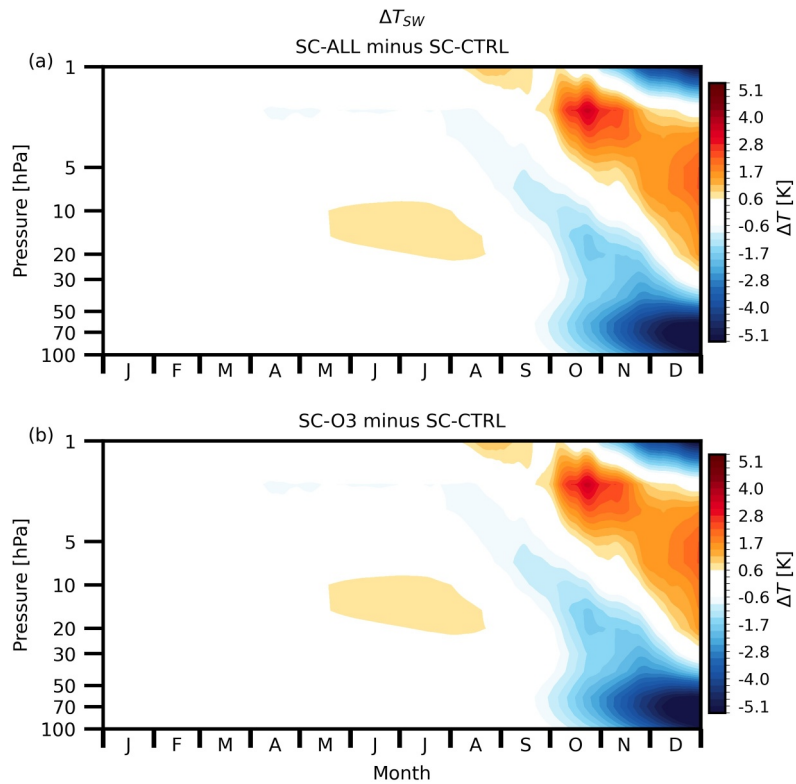

Figure 8. Time evolution of the polar cap-averaged temperature due to shortwave processes at all levels since 1 January 2022. Temperature differences between (a) SC-ALL and SC-CTRL runs, and (b) SC-O3 and SC-CTRL runs.

WACCM, while Zhang et al. (2024) focused on changes in stratospheric chemistry with a specified-dynamics version of WACCM.

Here, we extend their method, but focusing on decomposing the contributions of each forcing—ozone, water vapor, and sulfate aerosol—from the Hunga volcanic eruption to the simulated stratospheric circulation and temperature anomalies in 2022. To do so, we examined differences in climate anomalies based on a series of specified-chemistry WACCM experiments with various configurations of prescribed Hunga forcing.

The simulated climate responses to the Hunga forcing based on our specified-chemistry simulations (**SC-ALL**) show good agreement with previous coupled-chemistry simulations (**FR-ALL**). We find that the large-scale stratospheric cooling that occurred in 2022 austral winter/early spring (June–December) was mainly driven by changes in dynamical processes and not by direct radiative forcing. However, a key finding of this paper is that from October–December 2022, ozone's radiative feedback contributed to the prolonged cold temperature anomalies in the lower stratosphere (≈70 hPa) from October–December 2022 and hence to long lasting cold conditions of the polar vortex.

Together with findings from Wang et al. (2023) and Zhang et al. (2024), our results highlight that consistent model experiments with different configurations of a single model can improve our understanding of the climate responses associated with the observed volcanic eruption event. Our results also highlight some practical implications of using the Specified Chemistry setting of WACCM for studying climate and chemistry interactions. The similarity between the results from the FR and SC runs suggests that the SC runs can effectively estimate the temperature and circulation responses to the Hunga perturbations, providing a more computationally efficient alternative to fully coupled chemistry simulations (Smith et al., 2014). This efficiency makes SC runs useful for isolating the climate response to perturbations in individual chemical components.

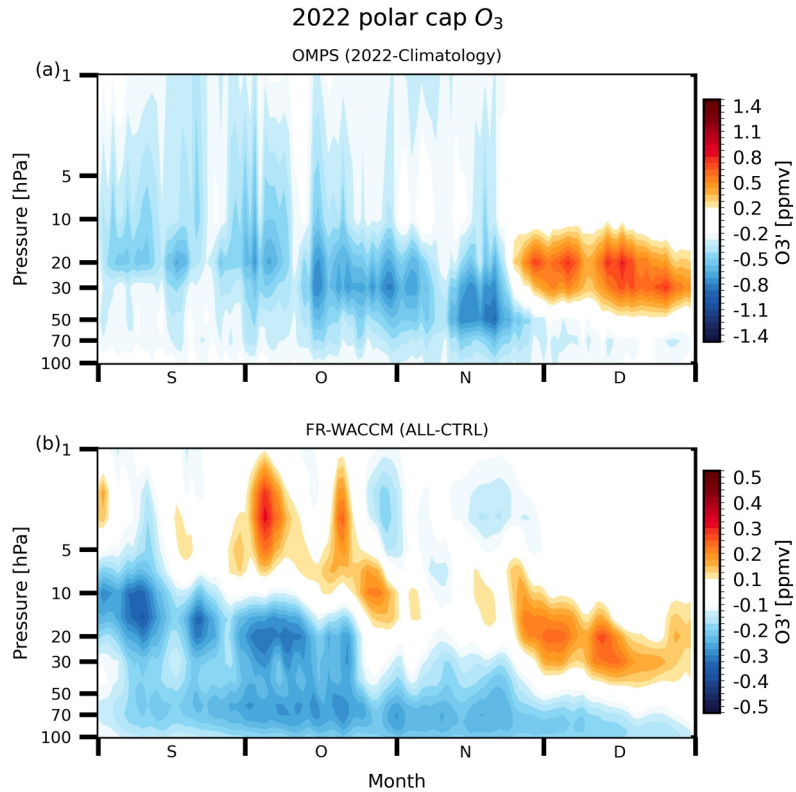

Figure 9. Springtime Southern Hemisphere polar cap-averaged (60°S–90°S) ozone anomalies (with respect to the 2012–2021 mean seasonal cycle) at all levels, based on (a) OMPS observations, and (b) FR-WACCM (FR-ALL minus FR-CTRL).

Data Availability Statement

Dataset used in the generation of the figures of this paper are available in Yook (2024). CESM2/WACCM6 is an open-source community model, which was developed with support primarily from the National Science Foundation, see Gettelman et al. (2019).

Acknowledgments

S. S and S. Y. are supported by Grants AGS-1906719 and AGS-2316980 from the Atmospheric Chemistry Division of the U. S. National Science Foundation (NSF) as well as a grant from the Future of Life Institute. The CESM project is supported primarily by the U.S. National Science Foundation. The authors acknowledge the Climate Simulation Laboratory at NCAR's Computational and Information Systems Laboratory (CISL; sponsored by NSF and other agencies) and the MIT's Massachusetts Green High Performance Computing Center (supported by the Center for Sustainability Science and Strategy) for providing computing and storage resources. We thank William Randel and the three anonymous reviewers for their helpful comments on the manuscript. Open Access funding enabled and organized by MIT Hybrid 2025.

References

Asher, E., Todt, M., Rosenlof, K., Thornberry, T., Gao, R.-S., Taha, G., et al. (2023). Unexpectedly rapid aerosol formation in the Hunga Tonga plume. *Proceedings of the National Academy of Sciences*, *120*(46), e2219547120. https://doi.org/10.1073/pnas.2219547120

Calvo, N., Garcia, R., & Kinnison, D. (2017). Revisiting Southern Hemisphere polar stratospheric temperature trends in WACCM: The role of dynamical forcing. *Geophysical Research Letters*, *44*(7), 3402–3410. https://doi.org/10.1002/2017gl072792

Calvo, N., Garcia, R. R., Marsh, D. R., Mills, M. J., Kinnison, D. E., & Young, P. J. (2012). Reconciling modeled and observed temperature trends over Antarctica. *Geophysical Research Letters*, *39*(16). https://doi.org/10.1029/2012gl052526

Carn, S., Krotkov, N., Fisher, B., & Li, C. (2022). Out of the blue: Volcanic SO2 emissions during the 2021–2022 eruptions of Hunga Tonga—Hunga Ha'apai (Tonga). *Frontiers in Earth Science*, *10*, 976962. https://doi.org/10.3389/feart.2022.976962

Coupe, J., & Robock, A. (2021). The influence of stratospheric soot and sulfate aerosols on the Northern Hemisphere wintertime atmospheric circulation. *Journal of Geophysical Research: Atmospheres*, *126*(11), e2020JD034513. https://doi.org/10.1029/2020jd034513

Coy, L., Newman, P. A., Wargan, K., Partyka, G., Strahan, S., & Pawson, S. (2022). Stratospheric circulation changes associated with the Hunga Tonga-Hunga Ha'apai eruption. *Geophysical Research Letters*, *49*(22), e2022GL100982. https://doi.org/10.1029/2022gl100982

DallaSanta, K., Gerber, E. P., & Toohey, M. (2019). The circulation response to volcanic eruptions: The key roles of stratospheric warming and eddy interactions. *Journal of Climate*, *32*(4), 1101–1120. https://doi.org/10.1175/jcli-d-18-0099.1

DallaSanta, K., & Polvani, L. M. (2022). Volcanic stratospheric injections up to 160 Tg (S) yield a Eurasian winter warming indistinguishable from internal variability. *Atmospheric Chemistry and Physics*, *22*(13), 8843–8862. https://doi.org/10.5194/acp-22-8843-2022

de Forster, P. M., & Shine, K. P. (1999). Stratospheric water vapour changes as a possible contributor to observed stratospheric cooling. *Geophysical Research Letters*, *26*(21), 3309–3312. https://doi.org/10.1029/1999gl010487

Fleming, E. L., Newman, P. A., Liang, Q., & Oman, L. D. (2024). Stratospheric temperature and ozone impacts of the Hunga Tonga-Hunga Ha'apai water vapor injection. *Journal of Geophysical Research: Atmospheres*, *129*(1), e2023JD039298. https://doi.org/10.1029/2023jd039298

Gelaro, R., McCarty, W., Suárez, M. J., Todling, R., Molod, A., Takacs, L., et al. (2017). The modern-era retrospective analysis for research and applications, version 2 (MERRA-2). *Journal of Climate*, *30*(14), 5419–5454. https://doi.org/10.1175/jcli-d-16-0758.1

Gettelman, A., Mills, M., Kinnison, D., Garcia, R., Smith, A., Marsh, D., et al. (2019). The whole atmosphere community climate model version 6 (WACCM6) [software]. *Journal of Geophysical Research: Atmospheres*, *124*(23), 12380–12403. https://doi.org/10.1029/2019JD030943

Khaykin, S., Podglajen, A., Ploeger, F., Grooß, J.-U., Tencé, F., Bekki, S., et al. (2022). Global perturbation of stratospheric water and aerosol burden by Hunga eruption. *Communications Earth and Environment*, *3*(1), 316. https://doi.org/10.1038/s43247-022-00652-x

Kodera, K. (1994). Influence of volcanic eruptions on the troposphere through stratospheric dynamical processes in the Northern Hemisphere winter. *Journal of Geophysical Research*, *99*(D1), 1273–1282. https://doi.org/10.1029/93jd02731

Kramarova, N., Nash, E., Newman, P., Bhartia, P., McPeters, R., Rault, D., et al. (2014). Measuring the antarctic ozone hole with the new Ozone Mapping and Profiler Suite (OMPS). *Atmospheric Chemistry and Physics*, *14*(5), 2353–2361. https://doi.org/10.5194/acp-14-2353-2014

Lu, J., Lou, S., Huang, X., Xue, L., Ding, K., Liu, T., et al. (2023). Stratospheric aerosol and ozone responses to the Hunga Tonga-Hunga Ha'apai volcanic eruption. *Geophysical Research Letters*, *50*(4), e2022GL102315. https://doi.org/10.1029/2022gl102315

Millan, L., Santee, M. L., Lambert, A., Livesey, N. J., Werner, F., Schwartz, M. J., et al. (2022). The Hunga Tonga-Hunga Ha'apai hydration of the stratosphere. *Geophysical Research Letters*, *49*(13), e2022GL099381. https://doi.org/10.1029/2022gl099381

Randel, W. J., Park, M., Wu, F., & Livesey, N. (2007). A large annual cycle in ozone above the tropical tropopause linked to the Brewer–Dobson circulation. *Journal of the Atmospheric Sciences*, *64*(12), 4479–4488. https://doi.org/10.1175/2007jas2409.1

Revell, L. E., Stenke, A., Luo, B., Kremser, S., Rozanov, E., Sukhodolov, T., & Peter, T. (2017). Impacts of Mt Pinatubo volcanic aerosol on the tropical stratosphere in chemistry–climate model simulations using CCMI and CMIP6 stratospheric aerosol data. *Atmospheric Chemistry and Physics*, *17*(21), 13 139–13 150. https://doi.org/10.5194/acp-17-13139-2017

Rieger, L., Randel, W., Bourassa, A., & Solomon, S. (2021). Stratospheric temperature and ozone anomalies associated with the 2020 Australian New Year fires. *Geophysical Research Letters*, *48*(24), e2021GL095898. https://doi.org/10.1029/2021gl095898

Robock, A. (2000). Volcanic eruptions and climate. *Reviews of Geophysics*, *38*(2), 191–219. https://doi.org/10.1029/1998rg000054

Robock, A., & Mao, J. (1995). The volcanic signal in surface temperature observations. *Journal of Climate*, *8*(5), 1086–1103. https://doi.org/10.1175/1520-0442(1995)008<1086:tvsist>2.0.co;2

Schoeberl, M., Wang, Y., Ueyama, R., Taha, G., & Yu, W. (2023). The cross equatorial transport of the Hunga Tonga-Hunga Ha'apai eruption plume. *Geophysical Research Letters*, *50*(4), e2022GL102443. https://doi.org/10.1029/2022gl102443

Schoeberl, M. R., Wang, Y., Ueyama, R., Taha, G., Jensen, E., & Yu, W. (2022). Analysis and impact of the Hunga Tonga-Hunga Ha'apai stratospheric water vapor plume. *Geophysical Research Letters*, *49*(20), e2022GL100248. https://doi.org/10.1029/2022gl100248

Sellitto, P., Podglajen, A., Belhadji, R., Boichu, M., Carboni, E., Cuesta, J., et al. (2022). The unexpected radiative impact of the Hunga Tonga eruption of 15th January 2022. *Communications Earth and Environment*, *3*(1), 288. https://doi.org/10.1038/s43247-022-00618-z

Smith, K. L., Neely, R., Marsh, D., & Polvani, L. M. (2014). The specified chemistry whole atmosphere community climate model (SC-WACCM). *Journal of Advances in Modeling Earth Systems*, *6*(3), 883–901. https://doi.org/10.1002/2014ms000346

Taha, G., Loughman, R., Colarco, P., Zhu, T., Thomason, L., & Jaross, G. (2022). Tracking the 2022 Hunga Tonga-Hunga Ha'apai aerosol cloud in the upper and middle stratosphere using space-based observations. *Geophysical Research Letters*, *49*(19), e2022GL100091. https://doi.org/10.1029/2022gl100091

Taha, G., Loughman, R., Zhu, T., Thomason, L., Kar, J., Rieger, L., & Bourassa, A. (2021). OMPS LP Version 2.0 multi-wavelength aerosol extinction coefficient retrieval algorithm. *Atmospheric Measurement Techniques*, *14*(2), 1015–1036. https://doi.org/10.5194/amt-14-1015-2021

Toohey, M., Krüger, K., Bittner, M., Timmreck, C., & Schmidt, H. (2014). The impact of volcanic aerosol on the Northern Hemisphere stratospheric polar vortex: Mechanisms and sensitivity to forcing structure. *Atmospheric Chemistry and Physics*, *14*(23), 13063–13079. https://doi.org/10.5194/acp-14-13063-2014

Ueyama, R., & Wallace, J. M. (2010). To what extent does high-latitude wave forcing drive tropical upwelling in the Brewer–Dobson circulation? *Journal of the Atmospheric Sciences*, *67*(4), 1232–1246. https://doi.org/10.1175/2009jas3216.1

Vömel, H., Evan, S., & Tully, M. (2022). Water vapor injection into the stratosphere by Hunga Tonga-Hunga Ha'apai. *Science*, *377*(6613), 1444–1447. https://doi.org/10.1126/science.abq2299

Wang, X., Randel, W., Zhu, Y., Tilmes, S., Starr, J., Yu, W., et al. (2023). Stratospheric climate anomalies and ozone loss caused by the Hunga Tonga-Hunga Ha'apai volcanic eruption. *Journal of Geophysical Research: Atmospheres*, *128*(22), e2023JD039480. https://doi.org/10.1029/2023jd039480

Witze, A. (2022). Why the Tongan eruption will go down in the history of volcanology. *Nature*, *602*(7897), 376–378. https://doi.org/10.1038/d41586-022-00394-y

Yook, S. (2024). Replication data for: Figures in the impact of 2022 Hunga Tonga-Hunga Ha'apai (Hunga) eruption on stratospheric circulation and climate [Dataset]. *Harvard Dataverse*. https://doi.org/10.7910/DVN/0RGYW8

Yu, P., Davis, S. M., Toon, O. B., Portmann, R. W., Bardeen, C. G., Barnes, J. E., et al. (2021). Persistent stratospheric warming due to 2019–2020 Australian wildfire smoke. *Geophysical Research Letters*, *48*(7), e2021GL092609. https://doi.org/10.1029/2021gl092609

Yu, W., Garcia, R., Yue, J., Smith, A., Wang, X., Randel, W., et al. (2023). Mesospheric temperature and circulation response to the Hunga Tonga-Hunga-Ha'apai volcanic eruption. *Journal of Geophysical Research: Atmospheres*, *128*(21), e2023JD039636. https://doi.org/10.1029/2023jd039636

Yulaeva, E., Holton, J. R., & Wallace, J. M. (1994). On the cause of the annual cycle in tropical lower-stratospheric temperatures. *Journal of the Atmospheric Sciences*, *51*(2), 169–174. https://doi.org/10.1175/1520-0469(1994)051<0169:otcota>2.0.co;2

Zawada, D. J., Rieger, L. A., Bourassa, A. E., & Degenstein, D. A. (2018). Tomographic retrievals of ozone with the OMPS Limb profiler: Algorithm description and preliminary results. *Atmospheric Measurement Techniques*, *11*(4), 2375–2393. https://doi.org/10.5194/amt-11-2375-2018

Zhang, J., Kinnison, D., Zhu, Y., Wang, X., Tilmes, S., Dube, K., & Randel, W. (2024). Chemistry contribution to stratospheric ozone depletion after the unprecedented water-rich Hunga Tonga eruption. *Geophysical Research Letters*, *51*(7), e2023GL105762. https://doi.org/10.1029/2023gl105762

Zhu, Y., Bardeen, C. G., Tilmes, S., Mills, M. J., Wang, X., Harvey, V. L., et al. (2022). Perturbations in stratospheric aerosol evolution due to the water-rich plume of the 2022 Hunga-Tonga eruption. *Communications Earth and Environment*, *3*(1), 248. https://doi.org/10.1038/s43247-022-00580-w

Zou, Y., Rasch, P. J., Wang, H., Xie, Z., & Zhang, R. (2021). Increasing large wildfires over the western United States linked to diminishing sea ice in the Arctic. *Nature Communications*, *12*(1), 6048. https://doi.org/10.1038/s41467-021-26232-9